No Warm-Phase Invigoration of Convection Detected during GoAmazon

RUSEN ÖKTEM,[a,b] DAVID M. ROMPS,[a,b] AND ADAM C. VARBLE[c]

[a] *Department of Earth and Planetary Science, University of California, Berkeley, Berkeley, California*
[b] *Climate and Ecosystem Sciences Division, Lawrence Berkeley National Laboratory, Berkeley, California*
[c] *Atmospheric Sciences and Global Change Division, Pacific Northwest National Laboratory, Richland, Washington*

(Manuscript received 21 November 2022, in final form 31 March 2023, accepted 6 April 2023)

ABSTRACT: It has been proposed that air pollution increases the updraft speeds of warm-phase convective clouds by reducing their supersaturation and, thereby, enhancing their buoyancy. Observations from the GoAmazon field campaign, sampled using subjective criteria, have been offered as evidence for this warm-phase invigoration. Here, we reexamine those GoAmazon observations using objective sampling criteria and find no indication that air pollution increases warm-phase updraft speeds. In addition, the observations yield no statistically significant relationship between aerosol concentrations and either moist-convective vertical velocity or reflectivity in either the lower or upper troposphere.

KEYWORDS: Deep convection; Aerosols; Aerosol indirect effect; Aerosol-cloud interaction

1. Introduction

The number concentration of atmospheric aerosols is observed to affect clouds via changes to their drop size distribution, which then alters many microphysical processes, with possible feedbacks to cloud dynamics (Tao et al. 2012; Fan et al. 2016). It has been hypothesized that characteristics such as cloud albedo, cloud depth, radar reflectivity, and flash rate are due, in part, to an effect of aerosol number concentration on moist convective updraft speeds (e.g., Andreae et al. 2004; Koren et al. 2005, 2010; Li et al. 2011; Yuan et al. 2011; Storer et al. 2014; Stolz et al. 2015; Hu et al. 2019). This proposed effect is referred to as aerosol invigoration of moist convection. Other studies have questioned the veracity of evidence for moist convective invigoration (e.g., Varble 2018; Grabowski 2018; Igel and van den Heever 2021) or pointed out complex dependencies on the state of the environment and clouds (e.g., Khain et al. 2008; Fan et al. 2009, 2016; Lebo 2018). Thus, the significance and magnitude of such an effect remains debated.

There are three hypotheses for how aerosols might increase updraft speeds. The hypothesis of "cold-phase invigoration" posits that higher aerosol concentrations augment updraft buoyancies by increasing the release of the latent heat of fusion, which is made possible by the suppression of rain and subsequent lofting of extra liquid to altitudes where it can freeze (Rosenfeld et al. 2008). It is noteworthy, however, that the increased condensate loading may offset the fusion effects on buoyancy (Grabowski and Morrison 2016; Igel and van den Heever 2021). The hypothesis of "humidity–entrainment invigoration" posits that higher aerosol concentrations lead to less precipitation and, therefore, more detrainment moistening of the environment, which then decreases entrainment-driven dilution of buoyancy in subsequent updrafts (Abbott and Cronin 2021). The hypothesis of "warm-phase invigoration," also referred as "condensational invigoration" (Cotton and Walko 2021), posits that higher aerosol concentrations lower liquid clouds' supersaturation, allowing updrafts to condense more water vapor, thereby releasing more latent heat and enhancing the updrafts' buoyancy (Fan et al. 2018, hereafter Fan18). But large values of supersaturation are required for the introduction of additional aerosols to generate noticeable increases in buoyancy and updraft speed (Igel and van den Heever 2021; Grabowski and Morrison 2021), and those large supersaturations are not well supported by observations (e.g., Romps et al. 2023).

Direct observational evidence for an effect of aerosols on updraft speeds is scant. Therefore, it was notable when Fan18 reported finding evidence for warm-phase invigoration in a correlation between boundary-layer aerosol number concentrations and free-tropospheric moist-convective updraft speeds. In particular, using data from the Green Ocean Amazon (GoAmazon) field campaign (Martin et al. 2016), they showed a greater correlation when ultrafine aerosol concentrations were included in addition to accumulation mode aerosols, which was interpreted as evidence of ultrafine aerosols nucleating as liquid drops, providing additional latent heating to warm (i.e., liquid) clouds, and thereby increasing the clouds' buoyancy and vertical velocity. Here, we evaluate the statistical significance of those correlations and assess whether they support the hypothesis of warm-phase invigoration.

We address three concerns about the analysis performed by Fan18. The first is that the methods described in Fan18 leave substantial room for subjectivity in choosing the time intervals used for averaging aerosol concentrations and for calculating quantiles of updraft speeds and reflectivities. Those subjective choices, which were not documented in Fan18, may have treated some storms differently from others, affecting the robustness of results. Here, we replicate (as closely as possible) those choices of Fan18 and show how the results change when an objective method is applied uniformly to all storms. The second concern is the reliance on a small number of convective events sampled with the "soda-straw" perspective of a vertically pointing Doppler radar. The resulting sampling error may lead

Corresponding author: Rusen Öktem, roktem@lbl.gov

DOI: 10.1175/JAS-D-22-0241.1

to correlations that appear to indicate a physical relationship, but that are not statistically significant. Here, we add analyses from a scanning radar, which sampled reflectivity over a much larger area, reducing the sampling error. Third, Fan18 did not analyze the properties of moist convection in the lower troposphere, which is where any warm-phase mechanism must operate, instead relying on correlations in the upper troposphere where ice was present. Here, we look for a warm-phase signal in the lower-tropospheric observations and evaluate its statistical significance. Concerns have also been expressed about the realism of Fan18's cloud-resolving simulations (Grabowski and Morrison 2020), but those simulations are not addressed here.

2. Data

The U.S. Department of Energy's Atmospheric Radiation Measurement (ARM) mobile facility was deployed 70 km to the west of Manaus, Brazil, for the GoAmazon campaign from January 2014 to November 2015. The campaign was designed to study the impact of industrial pollution from Manaus over the Amazon region, which has a background pollution close to preindustrial conditions during the wet season. Two GoAmazon instruments played a central role in the analysis of Fan18: the vertically pointing 1290-MHz radar wind profiler (RWP; Giangrande 2018) and the scanning mobility particle sizer (SMPS; Kuang et al. 2021).

The data stream from the RWP (*maorwpcls*)[1] (RWP; Giangrande 2018) includes the logarithm of reflectivity (variable *ReflectivityUAZR*), which is defined as $\mathrm{dB}Z \equiv 10\log_{10}(Z/Z_0)$, where Z is the best estimate of reflectivity and Z_0 is the reference reflectivity of air with one 1-mm-diameter drop per cubic meter. Also included in *maorwpcls* are the echo classification e (variable *EchoClassification*), rain rate r (variable *RainRateComputed*), and vertical velocity w (variable *VerticalVelocity*) (Giangrande et al. 2016). The echo classification specifies whether the radar measurement at the corresponding height and time is associated with "no significant echo," "stratiform with well-defined bright band," "stratiform without well-defined bright band," "melting layer," "stratiform freezing level," "convection," "weak convection," "cloud," or "Bragg and insects." dBZ, e, and w are available from 120 m to 17 km above ground level (AGL) in 120-m intervals every 6 s.

For this study, we analyze the same 17 deep-convective events (one on each of 17 different days) that Fan18 selected using the RWP dBZ data. Henceforth, these will be referred to as the 17 "days." These days occurred between 1 March and 31 May 2014, during the first intensive observation period of the GoAmazon campaign, and were selected by Fan18 based on the following criteria: 1) "convection occurred" between 1100 and 1900 local time, 2) no "convection occurred" during the 3 h preceding the "locally occurring systems," and 3) the maximum height of positive dBZ exceeds 10 km "for each event," but the terms in quotes were not defined in Fan18. We had difficulty interpreting these criteria in a way that would lead to the same set of days, but, for ease of comparison, we use here the same 17 days used by Fan18.

The second instrument used by Fan18 was the SMPS, which provided the concentration of boundary-layer aerosols and is available in data stream *maoaossmpsS1.b1* (SMPS; Kuang et al. 2021). The SMPS measures the aerosol size distribution for diameters D ranging from 10 to 500 nm, grouped in 104 bins, with adjacent bin boundaries related to each other by a factor of $10^{1/64}$. The size distributions are reported as averages over 5-min time intervals. Following Fan18, we calculate from these size distributions the number concentrations of aerosols with diameters greater than 15 nm (N_{15}; i.e., including ultrafine aerosols) and with diameters greater than 50 nm (N_{50}; i.e., excluding ultrafine aerosols).

To illustrate these two datasets, Fig. 1 plots the RWP and SMPS data for 26 March 2014, with dBZ and r in Fig. 1a and N_{15} and N_{50} in Fig. 1b. The vertical and horizontal lines indicate aspects of the sampling that will be discussed in the next section. All 17 days are shown in Fig. 1 and Figs. B1–B16 in appendix B. Figures B1–B16 have been displayed in increasing order of the representative N_{15} value assigned to each day by Fan18.

In addition to the data from the RWP and SMPS used by Fan18, we also include data from the Brazilian Sistema de Protecao da Amazonia S-band scanning precipitation radar (SIPAM; Schumacher and Funk 2018) in Manaus, which is available in data stream *sbmn_cappi*, version 2.0a. During the GoAmazon campaign, SIPAM provided plan projection indicator scans over several elevation angles at approximately 12-min time intervals. Those scans were mapped onto a fixed three-dimensional Cartesian grid, with spacings of 500 m in the vertical and 2 km in the horizontal up to an altitude of 20 km AGL (Schumacher and Funk 2018). The horizontal coverage extends out to a range of 240 km from the radar location in Manaus, thus encompassing the region between Manaus and the RWP. Aside from intermittent data loss around the time of deep convection on 17 and 21 March, SIPAM data are available continuously for all 17 days.

3. Methods

Fan18 calculated a representative aerosol concentration feeding the convection, a profile of convective velocity, and a profile of convective reflectivity, with velocity and reflectivity profiles representing the convective strength for each of the 17 days. They then showed correlations between the 17 pairs of profiles and the 17 aerosol concentrations. Given the large intraday fluctuations in aerosol concentrations and velocity/reflectivity profiles, special consideration must be given to choosing "representative" quantities in that type of analysis. In particular, for each of the 17 days, a time interval must be chosen over which to average the aerosol concentrations. Likewise, for each day, we must decide how and when to calculate the 90th percentiles of velocity and reflectivity. Here, we use four different methods for calculating those representative quantities: "Fan18Copy" (in which we take the aerosol concentrations from Table S1 of Fan18 and digitally extract the profiles of velocity and reflectivity from Figs. 2A and 2C

[1] Variable and data stream names shown in italics are the same names used in the ARM archive.

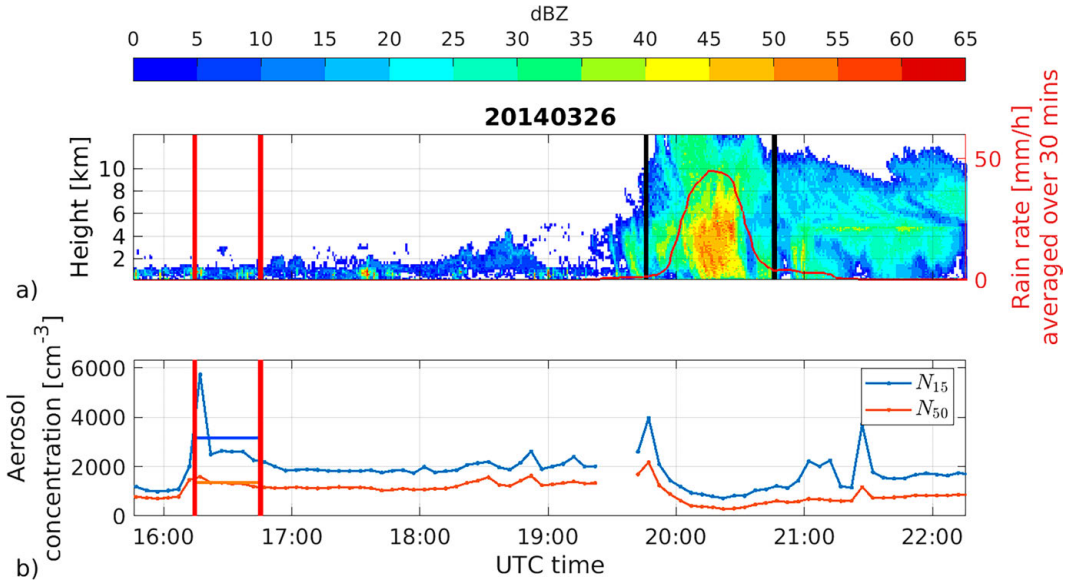

FIG. 1. (a) Reflectivity measured by the RWP on 26 Mar 2014 (20140326). The rain rate, smoothed by a half-hour moving window, is overlaid as a red curve (right axis). The black vertical bars indicate the 1-h window used in the Fan18Emulator method to calculate profiles of the 90th percentiles of updraft velocity and reflectivity. The red vertical bars mark the half-hour window for averaging aerosol concentration in the same test. (b) Aerosol concentrations N_{15} (blue) and N_{50} (orange). The blue and orange horizontal bars between the red bars show the aerosol concentrations listed in Table S1 of Fan18.

of Fan18), "Fan18Emulator" (in which we use the same data sources as Fan18 and try to replicate the results of Fan18 as closely as possible), "Objective" (in which we use the same data sources as Fan18, but apply a set of objective criteria for defining representative quantities), and "Scanning" (in which we use the same aerosol data as in the Objective method, but obtain reflectivity from a scanning precipitation radar instead of the vertically pointing RWP). The Fan18Copy method does not require further explanation, but summaries of the Fan18Emulator, Objective, and Scanning methods are given below; further details may be found in appendix A.

We will begin by describing the Fan18Emulator method, which is our attempt to replicate, as closely as possible, the results of Fan18. In Fan18, neither the time intervals used nor the methodology to pick them are reported, so we went searching for the time intervals that would most closely match the aerosol concentrations and velocity/reflectivity profiles presented in Fan18. In particular, we identified time intervals that 1) were consistent with the criteria described in Fan18 and/or inferred from personal communication (Y. Zhang 2021, personal communication) with the authors, 2) produced average aerosol concentrations that most closely matched those listed in Table S1 of Fan18, and 3) gave velocity and reflectivity profiles that most closely matched, by visual inspection, the data shown in Fig. 2 of Fan18. More detail on the Fan18Emulator method is given in section b of appendix A and the time intervals used in the method are listed in Table 1. Note that because we did not work closely with the authors of Fan18, their methodological choices are not fully known to us, and so there will be differences between the Fan18Emulator methods and the actual methods used by Fan18.

The velocity/reflectivity sampling intervals we found using the Fan18Emulator method are marked with vertical black bars in Figs. 1 and B1–B16. Similarly, our best-guess aerosol sampling intervals are marked with vertical red bars. The horizontal blue and orange bars show the average aerosol number concentrations listed in Table S1 of Fan18. These figures show that the aerosol sampling windows are very likely not consistent in terms of their proximity in time to the sampled convection, and the averages obtained are highly sensitive to the choice of sampling window. For example, in Fig. 1, it is not clear why it would make sense to choose an aerosol sampling window more than 3 h before the sampled deep convection and overlapping with a nonrepresentative spike in aerosol concentration. Shifting that averaging window later in time by 5 min would decrease the mean N_{15} by nearly 20%, while shifting the window later by an hour would decrease the mean N_{15} more than 1000 cm^{-3}. Thus, the sampling window choices can have a substantial impact on the results, possibly generating a signal where there is none.

To address this concern, we developed the Objective method, which defines objective criteria for selecting the sampling windows for both the aerosol concentrations and velocity/reflectivity profiles. In the Objective method, the criteria depend on parameters that can be varied over plausible ranges to give a measure of uncertainty. For each of the 17 days, we apply the Objective method with different sets of parameters as follows:

1) to generate a time series of convection, the reflectivity is averaged over either 2–5 or 2–7 km (2 combinations),
2) the time series of convection and the time series of rain are smoothed using either a 10- or 30-min centered averaging window (2 combinations),

TABLE 1. Sampling time intervals for aerosol (second column) and velocity and reflectivity (third column), and the values of N_{15} that are presented in Fan18 (fourth column) and calculated with the Fan18Emulator method (fifth column).

Date	N sampling intervals (UTC)	w and dBZ sampling intervals (UTC)	N_{15} in Fan18 (cm^{-3})	N_{15} by Fan18Emulator (cm^{-3})
22 Mar 2014	1642–1712	1733–1833	495	501
23 Mar 2014	1332–1402	1545–1645	553	550
21 Apr 2014	1601–1631	1701–1801	609	611
31 May 2014	1243–1313	1413–1513	711	601
30 May 2014	1333–1403	1600–1700	853	861
12 Apr 2014	1533–1603	1709–1809	1455	1449
16 May 2014	1613–1643	1713–1813	1525	1041
19 May 2014	1428–1458	1553–1653	1662	1772
23 Apr 2014	1721–1751	1800–1900	1721	1653
18 Apr 2014	1916–1946	2028–2128	1930	1938
1 Apr 2014	1403–1433	1632–1732	1998	1564
11 Mar 2014	1332–1402	1437–1537	2346	2695
20 May 2014	1548–1618	1621–1721	2679	2943
26 Mar 2014	1617–1647	1945–2045	3162	3053
20 Apr 2014	1526–1556	1841–1941	3462	3357
17 Mar 2014	1632–1702	1748–1848	3619	3590
21 Mar 2014	1902–1932	1935–2035	3848	3853

3) the time when convection starts and the time when the convection peaks are defined using those smoothed time series,
4) the aerosol concentrations are averaged over 30-, 60-, or 90-min time intervals that end 0-, 15-, 30-, or 60-min before the start of the convection ($3 \times 4 = 12$ combinations), and
5) the 90th-percentile profiles of velocity and reflectivity are calculated from 1-, 2-, 3-, 4-, or 6-h time intervals centered on the peak of convection (5 combinations).

This Objective method yields $2 \times 2 \times 12 \times 5 = 240$ sets of observations of each of the 17 days. For more detail on the Objective method, see section c of appendix A.

Like the Fan18Emulator method, the Objective method relies on the vertically pointing RWP, which samples a small volume of the atmosphere over the course of a day, raising the concern about sampling error. To address this, we designed our fourth and final method, which we refer to here as Scanning. The Scanning method uses the reflectivities obtained from the S-band scanning precipitation (SIPAM) radar. Since this radar is not looking vertically, it is not possible to obtain an estimate of vertical velocity, but it does provide reflectivity. This means that we can calculate a more representative 90th percentile of reflectivity using the SIPAM radar. To focus on the region around the RWP, which is located 70 km from the SIPAM radar, SIPAM data are collected over 60° of azimuth centered on the RWP and for radii ranging from 0 to 100 km. For its aerosol concentrations, the Scanning method uses the values obtained from the Objective method. For more detail on the Scanning method, see section d of appendix A.

4. Results

Fan18 presented two pieces of observational evidence in favor of warm-phase invigoration: a correlation between aerosol concentration and upper-tropospheric vertical velocity, and a correlation between aerosol concentration and reflectivity. We analyze each of these below.

a. Velocity

Figure 2a shows the profiles of updraft velocity digitized from the "$D > 15$ nm" panel of Fan18's Fig. 2B. Here, the label of "$D > 15$ nm" denotes that the aerosol number concentrations were calculated for all aerosols with diameters greater than 15 nm. We focus on Fan18's "$D > 15$ nm" results rather than their "$D > 50$ nm" results because their "$D > 50$ nm" results exhibited no systematic relationship between velocity/reflectivity profiles and aerosol concentrations.

The blue curve in Fig. 2a is an average over profiles from the days that had an aerosol concentration $N_{15} < 1000$ cm^{-3}, of which there were 5 days. Likewise, the other curves correspond to days with $1000 \le N_{15} < 1900$ cm^{-3} (cyan; 5 days in Fan18Emulator but 4 days in Fan18), $1900 \le N_{15} < 3000$ cm^{-3} (yellow; 3 days in Fan18Emulator but 4 days in Fan18), and $N_{15} \ge 3000$ cm^{-3} (red; 4 days). The shading around each curve shows the standard error digitized from Fig. 2B of Fan18. Note that the upper-tropospheric velocities increase with aerosol concentration. This was one of two pieces of observational evidence offered by Fan18 in support of warm-phase aerosol invigoration.

Our best effort at reproducing their profiles is shown in Fig. 2b, which uses the Fan18Emulator method. The shading around each curve indicates the uncertainty in the mean profile of each aerosol group, defined as plus and minus one standard deviation of the bootstrapped means. In bootstrapping, we treat each of the 17 days as an independent sample and draw 17 samples randomly with replacement 10 000 times. We found it impossible to replicate the profiles of Fan18Copy exactly. Nevertheless, we were able to find sampling windows that generate qualitatively similar results, with the four profiles sorted by their aerosol concentrations above an altitude of 8 km. The pertinent question is whether this result is robust or if it is a consequence of an idiosyncratic choice of sampling intervals.

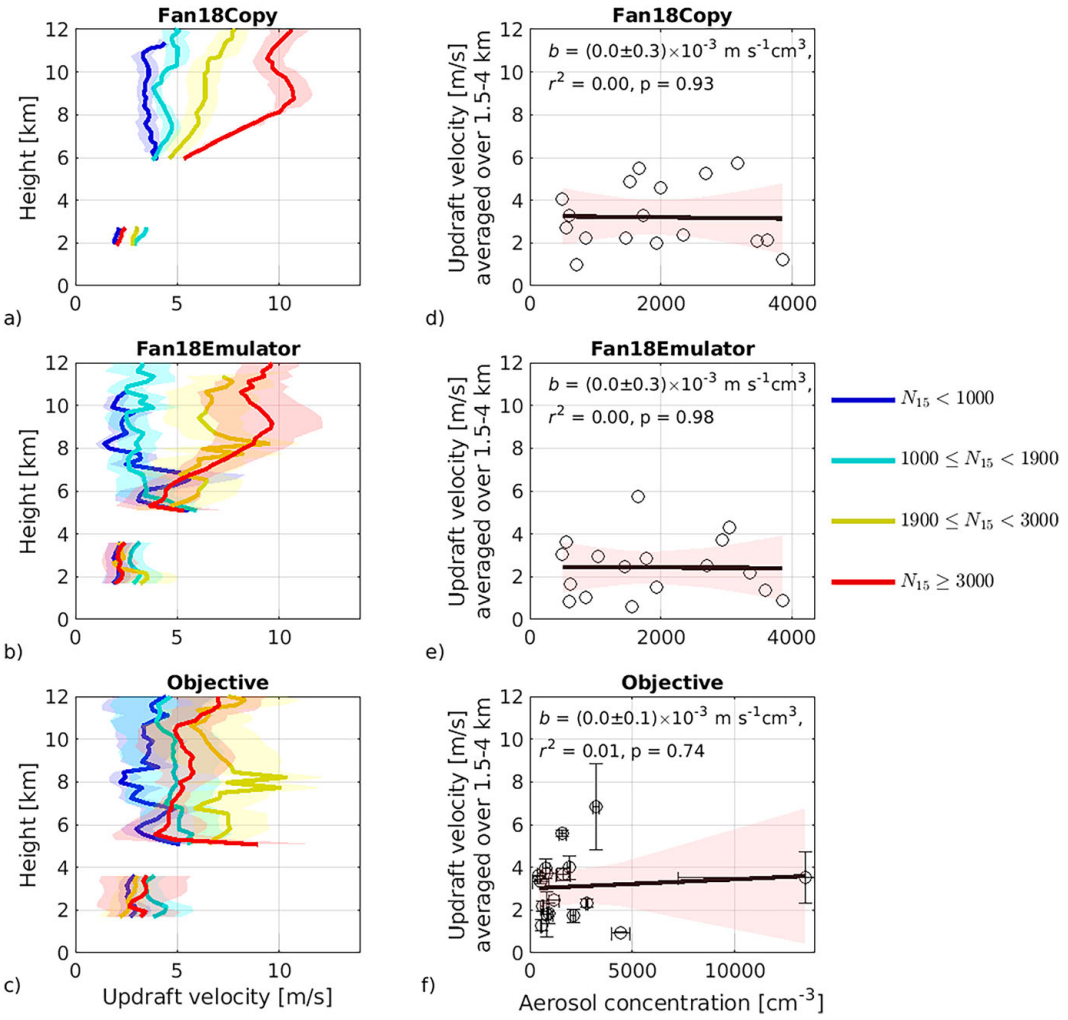

FIG. 2. (a)–(c) Averages of 90th-percentile updraft velocity profiles from days within each of four aerosol concentration ranges, indicated by blue ($N_{15} < 1000$ cm^{-3}), cyan ($1000 \le N_{15} < 1900$ cm^{-3}), yellow ($1900 \le N_{15} < 3000$ cm^{-3}), and red ($sN_{15} \ge 3000$ cm^{-3}). In (a), shading is the standard error calculated by Fan18 and is digitized from Fan18 Fig. 2B. In (c), the curves are calculated by averaging over 240 profiles of each aerosol concentration group. In (b) and (c), shading corresponds to the standard deviation calculated by bootstrapping. (d)–(f) For each of the 17 days, the 90th-percentile velocity profile averaged over the lower troposphere (1.5–4 km) plotted against the aerosol concentration. The black lines show the linear least squares fit with the slope b. The light red shading illustrates the 95% confidence interval band in the t test. The square of the Pearson correlation coefficient r^2 and the p value are printed at the top of the panels. The vertical and the horizontal error bars in (f) correspond to standard deviations among the multiple parameter settings of the Objective tests. The scanning radar does not measure vertical velocity; therefore, there are no panels for the scanning radar.

To evaluate this, we use the Objective method to generate the profiles shown in Fig. 2c. For each of the 240 different parameter sets described in section 3, we generate four updraft velocity profiles associated with the same four aerosol concentration ranges as in Fan18Copy and Fan18Emulator. Each solid curve in Fig. 2c is the mean of these 240 profiles of the corresponding aerosol group. The shading is plus and minus one standard deviation of bootstrapped means. For the Objective method, we bootstrap 10 000 times for each parameter set, generating 240 × 10 000 bootstrapped sets in total.

Unlike Fan18Copy and Fan18Emulator, the Objective results in Fig. 2c exhibit no systematic relationship between updraft velocity and aerosol concentration in the upper troposphere. Although the average updraft velocity for the group with the lowest aerosol concentrations (blue) is smaller than the averages of the other three groups through much of the upper troposphere, the uncertainties (shadings) show that this is not robust. The lack of a statistically significant relationship between updraft velocity and aerosol concentration in the upper troposphere is also confirmed by a regression analysis. If each day's average upper-tropospheric updraft velocity is

plotted against its average aerosol concentration, the p value goes from <0.05 in Fan18Copy and Fan18Emulator to 0.64 in Objective (see Fig. B18). Thus, it appears that the signal presented by Fan18 was an artifact of the choice of sampling intervals.

Although we see no evidence of aerosol invigoration in the upper troposphere, Fan18 claimed to be seeing warm-phase aerosol invigoration, which, if present, should generate a signal in the lower troposphere. But there is no signal in the lower troposphere visible in Figs. 2a–c. To check this, we can make a scatterplot of individual days. Starting with Fan18Copy, Fig. 2d plots each of the 17 days on two axes: updraft velocity averaged over 1.5–4 km (digitized from the "$D > 15$ nm" panel in Fan18's Fig. 2A) and the day's representative N_{15} aerosol concentration (from Fan18's Table S1). The squared Pearson correlation coefficient r^2 indicates the fraction of the variance explained by the data, the p value indicates the statistical significance, and the least squares regression slope b indicates the magnitude of the relationship, all of which are overlaid in the top of the panel. The 95% confidence interval (CI) bands in the t tests are displayed with the red shading in the plot.

We see from Fig. 2d that there is no signal: $r^2 = 0.00$, which indicates that there is no correlation between the aerosol concentration and lower-tropospheric updraft speeds. The best-fit slope is 0.0 ± 0.3 m s^{-1}(1000 cm^{-3})$^{-1}$, with 0.3 m s^{-1}(1000 cm^{-3})$^{-1}$ being the standard error. In other words, these data do not indicate any warm-phase invigoration. Instead, they rule out a large effect: they tell us that an increase in aerosol concentration of 1000 cm^{-3} is unlikely to coincide with a change of lower-troposphere updraft velocity greater in magnitude than 0.3 m s^{-1}, and very unlikely to be greater than 1 m s^{-1}. This is also consistent with the findings of Lebo (2014), who shows that changes in low-level aerosol loading (i.e., below 3 km) lead to negligible changes in mean convective updraft mass flux via warm phase invigoration below 7 km. Figures 2e and 2f show the results obtained from the Fan18Emulator and Objective methods, with the error bars on each point in Fig. 2f denoting the standard deviation among the 240 Objective parameter sets. As in Fan18Copy, there is no signal: Fan18Emulator and Objective have r^2 of 0.00 and 0.01, respectively, and best-fit slopes of 0.0 ± 0.3 m s^{-1}(1000 cm^{-3})$^{-1}$ and 0.0 ± 0.1 m s^{-1}(1000 cm^{-3})$^{-1}$, respectively. We see, therefore, that there is no evidence for warm-phase aerosol invigoration in these data.

Note that the range of the abscissa in Fig. 2f (Objective) is larger than in Fig. 2d (Fan18Copy) and Fig. 2e (Fan18Emulator). This is because of the time series of aerosol concentrations on 17 March. On that day, the boundary-layer aerosol concentration dropped from over 20 000 cm^{-3} to under 4000 cm^{-3} in an hour, associated with the first precipitation event; see Fig. B15. Fan18 measure the aerosol concentration between the two precipitation events (getting an aerosol concentration of 3619 cm^{-3}), while the Objective method more often than not measures the aerosol concentration before the first precipitation event, which is why the highest measured aerosol concentration in the Objective tests is so much higher. Excluding 17 March from the scatterplot in Fig. 2f, we would get $r^2 = 0.00$ and the best-fit slope would still be effectively zero at a value of 0.1 ± 0.4 m s^{-1}(1000 cm^{-3})$^{-1}$.

b. *Reflectivity*

The other piece of evidence that Fan18 presented was an observed relationship between aerosols and reflectivity. Figure 3a reproduces data digitized from the "$D > 15$ nm" panel of Fan18's Fig. 2C, which shows profiles of reflectivity averaged over the same aerosol ranges used in Figs. 2a–d. In addition to being ordered in the upper troposphere from low N_{15} to high N_{15}, the signal is large: the difference between the blue and red profiles, averaged over 5.5–12 km, is $\Delta\mathrm{dB}Z = 15$.

The reflectivity profiles from the Fan18Emulator method, shown in Fig. 3b, bear a broad resemblance to the Fan18Copy profiles, but do not match in detail. Nevertheless, the profiles are ordered the same as in Fan18Copy. Another way to see the relationship between aerosols and upper-tropospheric reflectivity is to average each day's profile of 90th-percentile reflectivity over 5.5–12 km and plot that against the day's representative aerosol concentration. The daily reflectivity data were not presented in Fan18, but we can make this plot using the Fan18Emulator method, which gives the relationship shown in Fig. 3f. Here, we see that the sampling windows used by Fan18 give a strong correlation with $r^2 = 0.53$ and a p value of 10^{-3}.

As before, we should ask if this result stems from an idiosyncratic choice of sampling windows. Repeating the analysis with the Objective method, we get the profiles shown in Fig. 3c. We see that these profiles exhibit less spread compared to Fan18Copy: the average over 5.5–12 km of the maximum spread in these profiles is $\Delta\mathrm{dB}Z = 6.5$, i.e., less than half the spread exhibited in Fan18. Furthermore, the profiles do not have a monotonic ordering with respect to aerosol concentration. Averaging the 90th-percentile reflectivity profiles from each day over 5.5–12 km and plotting against the representative aerosol concentration, Objective gives the relationship shown in Fig. 3g. We see that there is no statistically significant correlation (p value of 0.22) between reflectivity and aerosol concentration.

Repeating the analysis with the Scanning method gives the profiles in Fig. 3d. For 21 March, the scanning radar was not operating from 1725 to 2200 UTC, and the method did not catch enough (fewer than 10) samples to generate a reflectivity profile for that day from the rest of the scans. As a result, the Scanning method uses 16 out of the 17 days. These profiles have an even smaller spread: the average over 5.5–12 km of the maximum spread in these profiles is $\Delta\mathrm{dB}Z = 4.8$. Notably, the spread in reflectivity in the lower troposphere is reduced close to zero using the scanning radar. The lower-tropospheric updraft velocities, discussed in section 4a, are what most directly demonstrate an absence of any detectable warm-phase invigoration, but the Scanning method's lack of any lower-tropospheric reflectivity signal is consistent with that result.

Taken together, the Objective and Scanning profiles in Figs. 3c and 3d suggest that the large spread in Fan18 is due to a combination of the chosen sampling windows and sampling error from the vertically pointing RWP. Averaging the 90th-percentile reflectivity profiles from each day over 5.5–12 km and plotting against the representative aerosol concentration, Scanning gives the relationship shown in Fig. 3h. Again, there

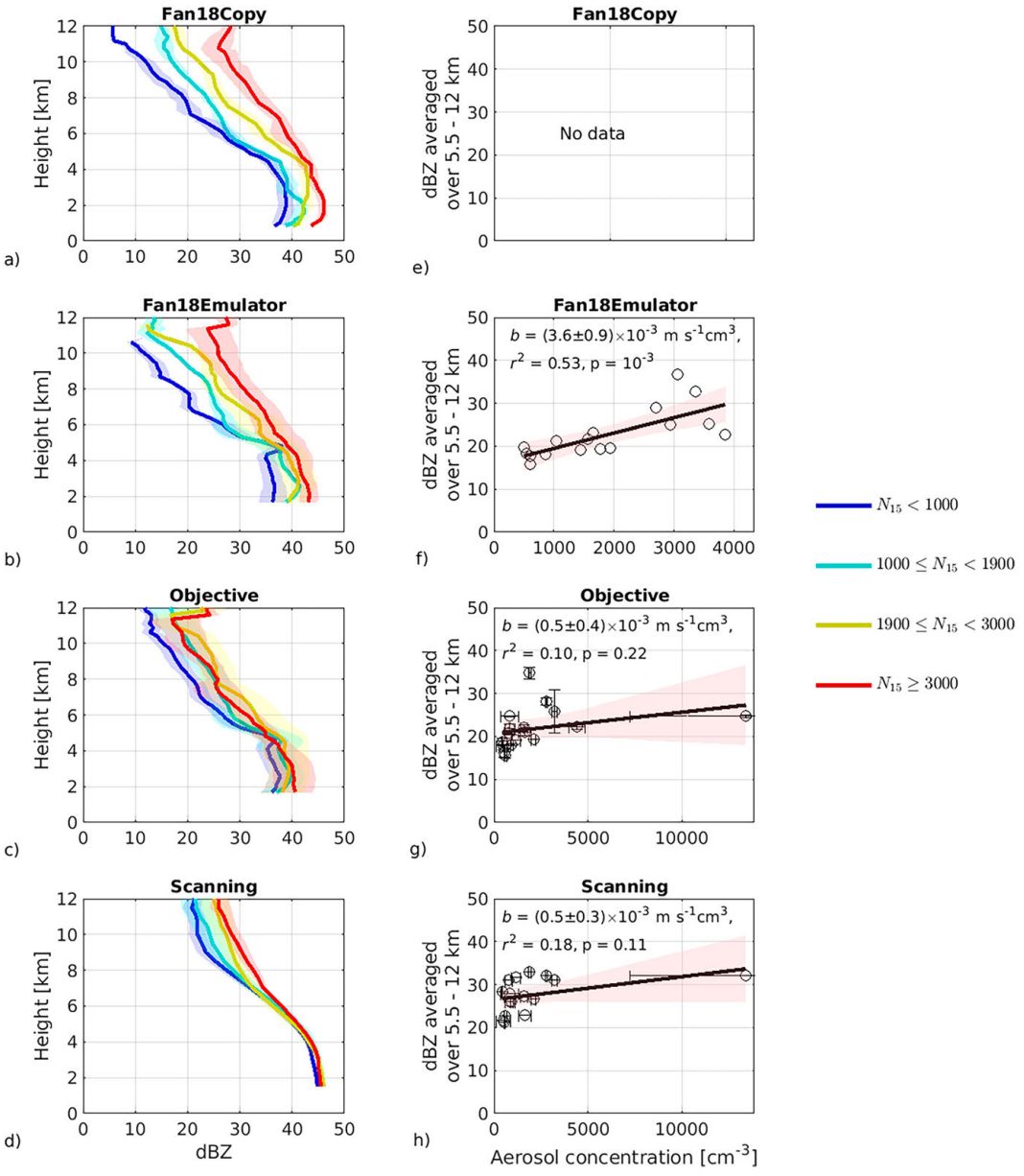

FIG. 3. (a)–(d) Reflectivity profiles averaged over the days within each of the four aerosol concentration ranges, which are the same as in Fig. 2. In (a), shading is the standard error calculated by Fan18 and is digitized from Fan18 Fig. 2C. In (c), the curves are calculated by averaging over 240 profiles of each aerosol concentration group. In (b)–(d), shading corresponds to the standard deviation calculated by bootstrapping as in Fig. 2. (e)–(h) For each of the 17 days, the reflectivity averaged over the upper troposphere (5.5–12 km) plotted against the representative aerosol concentration. The black lines show the linear least squares fit with the slope b. The light red shading illustrates the 95% CI band in the t test. The square of the Pearson correlation coefficient r^2 and the p value are printed at the top of the panels. The vertical and the horizontal error bars in (g) and (h) correspond to standard deviations among the multiple parameter settings of the Objective tests. The plot in (e) is blank because reflectivity values for Fan18Copy are not available separately for each day.

is no statistically significant correlation ($p = 0.11$) between reflectivity and aerosol concentration.

If 17 March were treated as an outlier and excluded from the scatterplot in Fig. 3g, the Objective method would give $r^2 = 0.23$ and a p value of 0.05, just barely significant at the 5% level. Likewise, excluding 17 March from the Scanning scatterplot in Fig. 3h, we get $r^2 = 0.29$ and a p value of 0.03. Thus, we see that we can generate a barely significant relationship between aerosol concentrations and upper-tropospheric reflectivity, but only if 17 March is excluded

from the analysis. We conclude, therefore, that the data from this limited number of days are suggestive of a relationship, but are not conclusive. It is possible that a greater number of days could demonstrate a statistically significant correlation, in which case the next step would be to look for confounding variables.

5. Discussion

It is important to note that a relationship between upper-tropospheric reflectivity and aerosol concentration, even if present, does not imply the existence of any warm-phase invigoration. In fact, we have already seen from Figs. 2d–2f that there is no signal of warm-phase invigoration. Instead, a correlation between upper-tropospheric reflectivity and aerosol concentration could be a consequence of a different aerosol-invigoration mechanism, such as cold-phase or humidity–entrainment invigoration. Or, it could be caused by an effect of aerosols on the microphysics (e.g., altered properties of supercooled liquid changing mixed-phase ice growth) without any increase in updraft speeds. Or, it could be a noncausal correlation if aerosol concentrations and convective activity covary with some other aspect of the mesoscale or synoptic state. Regarding the hypothesis of a noncausal correlation, it is worth noting that the three days that consistently fall into the lowest aerosol range (Figs. B2–B4) are among the five days with the lowest most unstable convective available potential energy (MUCAPE; computed at the same time for all days from the morning soundings).[2] Likewise, there is a positive correlation between MUCAPE and lower-tropospheric updraft velocity in the Objective method (Fig. B19), with a best-fit slope of 1 m s^{-1} per kJ of MUCAPE. The relationships between MUCAPE and velocity/reflectivity are not statistically significant, but that is expected given the substantial spatiotemporal variability in CAPE and the limited days of observations. Nevertheless, such relationships could still contribute to correlations of aerosol concentration with updraft velocity and convective radar reflectivity.

Note that we have presented results only for N_{15} because that was the measure of aerosol concentration that gave the most compelling results in Fan18. In the Objective method, both N_{15} and N_{50} give statistically insignificant correlations between aerosol concentration and velocity/reflectivity. This is illustrated by Fig. B17, which shows the Objective profiles of velocity calculated using N_{50}.

[2] In Fan18, all 17 days are listed as having similar CAPE/CIN values, when soundings closest to the peak in convection are considered. However, their computed CAPE values appear to be too high (see the "CAPE-Fan18" column in Table B1), potentially due to soundings being initialized with suspiciously high values of near-surface temperature and dewpoint taken from a meteorological station, which we have removed such that only radiosonde measurements from about 10-m height and upward are used. In addition, only some days have soundings later in the day, and since CAPE increases as the day proceeds, mixing morning and afternoon soundings can lead to erroneous conclusions.

6. Summary

Using data from the GoAmazon campaign, Fan18 claimed that warm-phase invigoration had caused deep-convective updraft speeds and reflectivities to be higher in the presence of a higher concentration of aerosols. Using the same data, we find no evidence of warm-phase invigoration; to the contrary, the data seem to rule out any strong warm-phase invigoration effect. The data hint at a correlation between boundary-layer aerosol concentration and moist-convective reflectivity in the upper troposphere, but the correlation is not statistically significant. Even if a correlation is present in reality, it could be generated by multiple mechanisms other than warm-phase invigoration, including a different invigoration mechanism, a direct effect of aerosols on microphysics (without any invigoration), or a noncausal correlation that aerosols and updrafts share with the synoptic or mesoscale meteorology.

There appear to be two reasons for the false positive in Fan18. The first is the specific selection of time intervals for calculating representative aerosol concentrations and velocity/reflectivity profiles. The statistical significance in Fan18 is eliminated using objective criteria for selecting those time intervals. The second is sampling error from using a vertically pointing radar, which is confined to a "soda-straw" view of the atmosphere. Using a scanning radar reduces the variance in the reflectivity profiles and produces essentially zero covariance between aerosol concentrations and lower-tropospheric reflectivity.

Acknowledgments. This work was supported by the U.S. Department of Energy's Atmospheric System Research program through the Office of Science's Biological and Environmental Research program under Contract DE-AC02-05CH11231. Observational data were obtained from the Atmospheric Radiation Measurement (ARM) user facility, a U.S. Department of Energy (DOE) Office of Science user facility managed by the Biological and Environmental Research program.

Data availability statement. RWP, SIPAM, and SMPS data used in this study are from GoAmazon field campaign MAO site and they are openly available from the Atmospheric Radiation Measurement (ARM) Data Center at https://doi.org/10.5439/1440997 (accessed on 23 November 2021), https://doi.org/10.5439/1459573 (accessed on 23 November 2021), and https://doi.org/10.5439/1476898 (accessed on 14 October 2022), respectively.

APPENDIX A

The Four Methods

Further details are given here on the four methods used to calculate aerosols and velocity/reflectivity profiles.

a. Fan18Copy

In the Fan18Copy method, all of the data are extracted directly from the figures and tables of Fan18. The representative

aerosol concentrations for each of the 17 days are taken from Fan18's Table S1. The velocity and reflectivity profiles are digitized from Fan18's Figs. 2A and 2C. Unless noted otherwise, we use data from the "$D > 15$ nm" panels of those figures.

b. Fan18Emulator

The Fan18Emulator method is our best effort to replicate the results of Fan18, although note that we did not work closely with the authors of Fan18 and so we did not have all of the information necessary to exactly reproduce their analysis. Fan18 generated the representative velocity/reflectivity profiles for a given day using the 2–3 h time window containing the strongest peak as determined by inspection of the RWP data (Y. Zhang 2021, personal communication). Because the sampling intervals used by Fan18 are not documented in Fan18, we attempt to replicate their results by first defining t_p as the time when convection peaks in intensity. To this end, we generate a one-dimensional $\overline{\mathrm{dB}Z}(t)$ as follows:

$$\overline{\mathrm{dB}Z}(t) = \frac{1}{\Delta t(h_2 - h_1)} \int_{t-\Delta t/2}^{t+\Delta t/2} dt \int_{h_1}^{h_2} dz\, \mathrm{dB}Z(z, t)\mathcal{H}[\mathrm{dB}Z(z, t)], \tag{A1}$$

where $\mathcal{H}$ is the Heaviside unit step function and h_1, h_2, and Δt are parameters of the method. For the Fan18Emulator method, these take values of $h_1 = 2$ km, $h_2 = 7$ km, and $\Delta t = 30$ min. We also define a measure of convection C as

$$C(t) = \begin{cases} 1 & e(z, t) = \text{convection} \quad \forall\ z \text{ such that } h_1 \le z \le h_2 \\ 0 & \text{otherwise} \end{cases}, \tag{A2}$$

where e is the EchoClassification variable in the RWP dataset. For any given day, the time of peak convection t_p is defined as the time when $C\overline{\mathrm{dB}Z}$ is maximal. To define representative velocity/reflectivity profiles, we focused on a sampling window centered on t_p. We tried durations of 1, 2, and 3 h for this sampling window, but we settled on 1 h because this gave, by visual inspection, the closest agreement with Fig. 2 of Fan18. Averaging the updraft velocities and reflectivities over their 90th–100th percentiles, which was the stated methodology of Fan18, gave profiles that were much noisier than shown in the figures of Fan18. Therefore, we generated the representative profiles of velocity by taking the 90th percentile at each height within that sampling window, and likewise for reflectivity. At heights where there were fewer than twenty-five 6-s values of velocity within the sampling window, we left the 90th-percentile profile undefined, and likewise for reflectivity.

Next, we try to replicate the aerosol number concentrations listed in Table S1 of Fan18 by averaging over a half-hour window as described in Fan18. We learned through personal communication (Y. Zhang 2021, personal communication) that Fan18 chose a 0.5 h averaging window within 2 h prior to the time when $\mathrm{dB}Z > 0$ reaches above 4 km height and during conditions as close to clear sky as possible. Fan18 states that aerosols were averaged right before convective clouds occurred at the GoAmazon T3 site, but the aerosol sampling window appears to sometimes be about 3 h before the sampled reflectivity and vertical velocities (see Figs. 1 and B14). Therefore, their half-hour aerosol concentration sampling window may start anywhere over a wide range of times before t_p. To match Fan18 results for a given day, we look for the half-hour window during that day that has no convection deeper than 4 km (either $\mathrm{dB}Z < 0$ at some height from 2 to 4 km or $\mathrm{dB}Z < 0$ at all heights above 4 km), precedes the convective sampling window (meaning that the half hour ends before the 1-h interval straddling t_p), and in which $(\Delta N_{15})^2 + (\Delta N_{50})^2$ is minimized, where $\Delta N_X = N_X^{\mathrm{Fan18Emulator}} - N_X^{\mathrm{Fan18}}$ and N_X^{Fan18} is taken from Table S1 of Fan18. Despite these efforts, we were unable to replicate the values listed in that table. Our calculations matched the corresponding entries in Table S1 of Fan18 to within 15% relative error for all but 4 days. For 31 May (Fig. B4), 16 May (Fig. B7), 19 May (Fig. B8), and 1 April (Fig. B11), we were only able to match the value of $\overline{N}_{15}$ ($\overline{N}_{50}$) listed in Table S1 of Fan18 to within relative errors of 15% (44%), 32% (48%), 7% (30%), and 22% (26%), respectively.

c. Objective

The Objective method defines the sampling windows for aerosols and convective profiles based on objective criteria. The peak of convection is defined as the time when $C\overline{\mathrm{dB}Z}$ is maximized, with $\overline{\mathrm{dB}Z}$ and C defined as in Eqs. (A1) and (A2). For a given day, we define $\bar{r}$ as the time series of rain rate r smoothed with a centered averaging window of width Δt,

$$\bar{r}(t) = \frac{1}{\Delta t} \int_{t-\Delta t/2}^{t+\Delta t/2} dt\, r(t). \tag{A3}$$

We then define the start time of convection t_c as the earliest time such that both $\overline{\mathrm{dB}Z} > 5$ and $\bar{r} > 1\,\mathrm{mm\,h^{-1}}$ for all times between t_c and t_p. For a given day, we calculate an average aerosol concentration and profiles of velocity and reflectivity 240 different ways:

1) for the purposes of defining t_p and t_c, h_1 is set to 2 km, h_2 is set to either 5 or 7 km, and Δt is set to either 10 or 30 min (4 combinations),
2) the representative aerosol concentration is calculated as a mean over 30-, 60-, or 90-min time intervals that end 0-, 15-, 30-, or 60-min before t_c (12 combinations), and
3) the profiles of the 90th percentiles of velocity and reflectivity are calculated as described in the Fan18Emulator method, but using 1-, 2-, 3-, 4-, or 6-h time intervals centered on t_p (5 combinations).

The above parameter sets reflect a systematic and replicable way of generating $4 \times 12 \times 5 = 240$ objective ways of quantifying aerosol loading and convection strength. While testing with these parameter sets, we checked if the aerosol averaging window coincided with another (weaker) convection ($\mathrm{dB}Z > 0$ simultaneously somewhere between 2 and 4 km and somewhere above 4 km) and discard that day from the test when it occurred. This resulted in eliminating one of the 17 days in 70 of the 240 tests.

d. Scanning

The Scanning method uses the same aerosol concentrations calculated in the Objective method but uses reflectivity from the scanning precipitation radar (SIPAM) instead of from the vertically pointing RWP. The SIPAM radar is located approximately 70 km east-northeast of the GoAmazon T3 site, where RWP and SMPS are located. The SIPAM radar measures reflectivity over an area that includes the T3 site. To reduce sampling error while still focusing on the same convection, we restrict attention to SIPAM dBZ sampled in a 60° azimuthal sector centered on the T3 site and out to a radial distance of 100 km from the SIPAM radar. When collecting reflectivity from that sector, we exclude stratiform precipitation using a convective mask following Steiner et al. (1995). We generate a vertical reflectivity profile for each day by calculating the 90th percentile at each height of positive convective dBZ samples within the specified sector and time interval from 1500 to 2300 UTC.

APPENDIX B

Supplemental Figures

This appendix presents supplemental figures. RWP and SMPS data are plotted for 16 deep-convective events in Figs. B1–B16. Figure B17 shows the Objective profiles of velocity calculated using N_{50}. In Fig. B18, each day's average upper-tropospheric updraft velocity is plotted against its average aerosol concentration. In Fig. B19, each day's average lower-tropospheric updraft velocity and upper-tropospheric reflectivity are plotted against its MUCAPE. Finally, Table B1 lists each day's CAPE, MUCAPE, and MUCIN values.

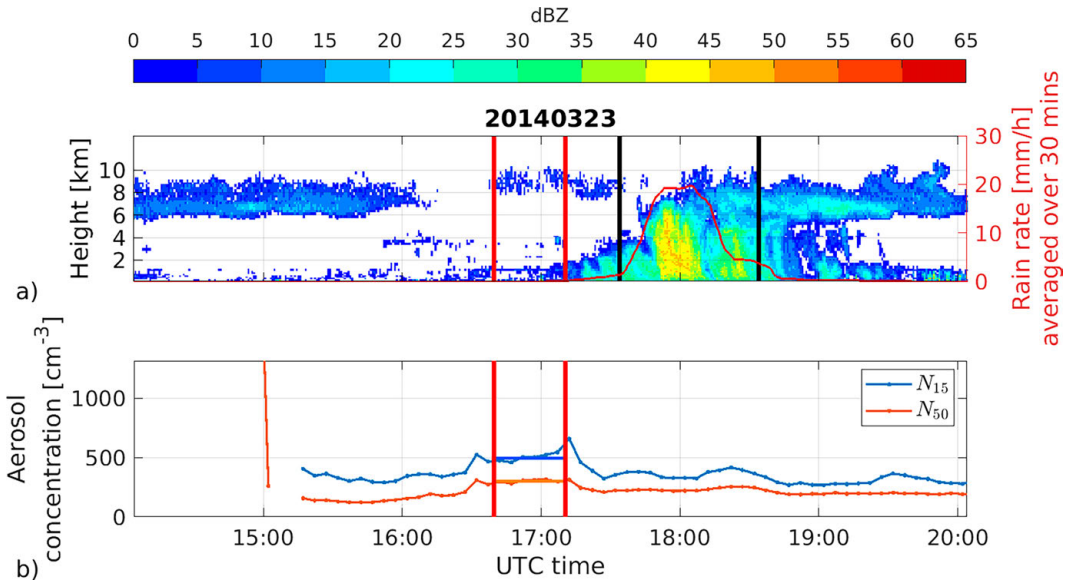

FIG. B1. As in Fig. 1, but for 23 Mar 2014. Figures B1–B16 are presented in increasing order of the representative N_{15} value assigned to each day by Fan18.

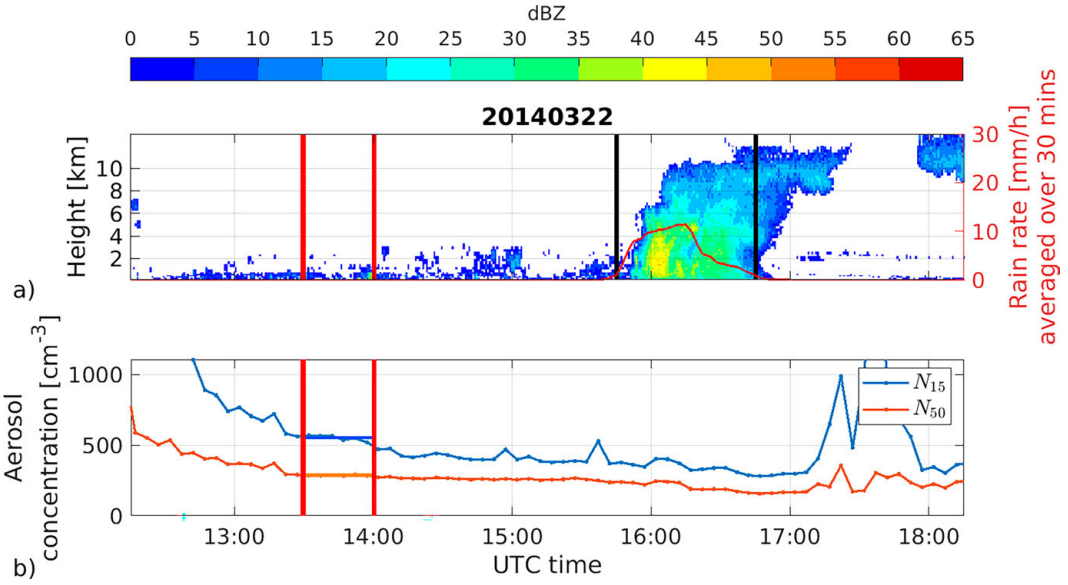

FIG. B2. As in Fig. 1, but for 22 Mar 2014.

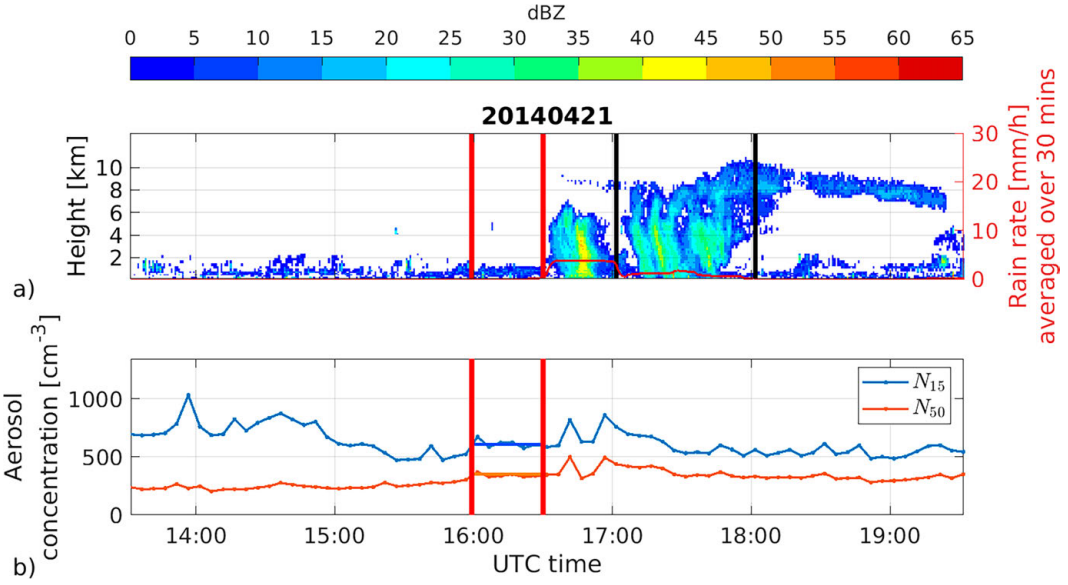

FIG. B3. As in Fig. 1, but for 21 Apr 2014.

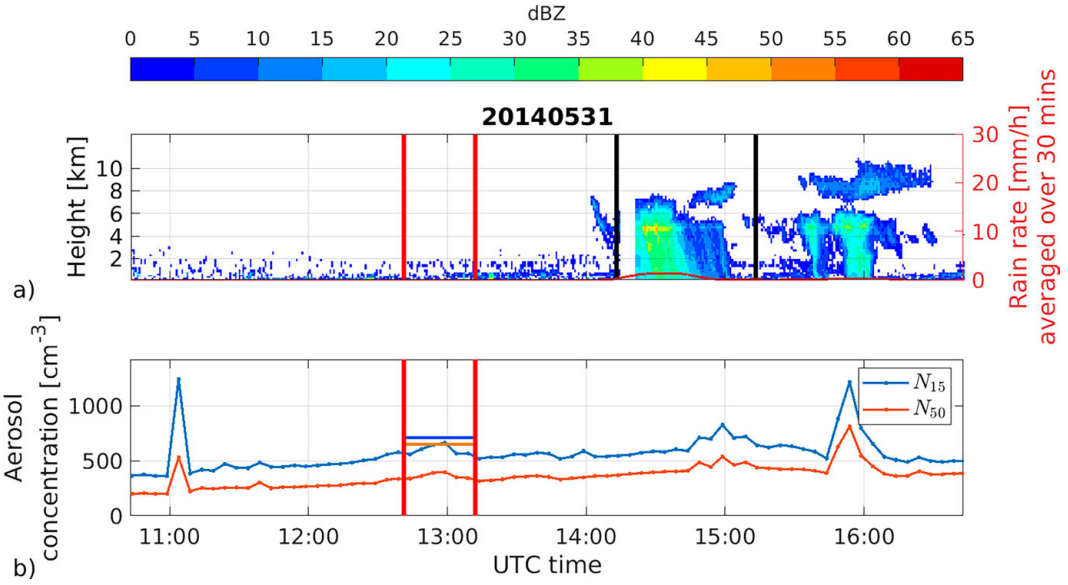

FIG. B4. As in Fig. 1, but for 31 May 2014.

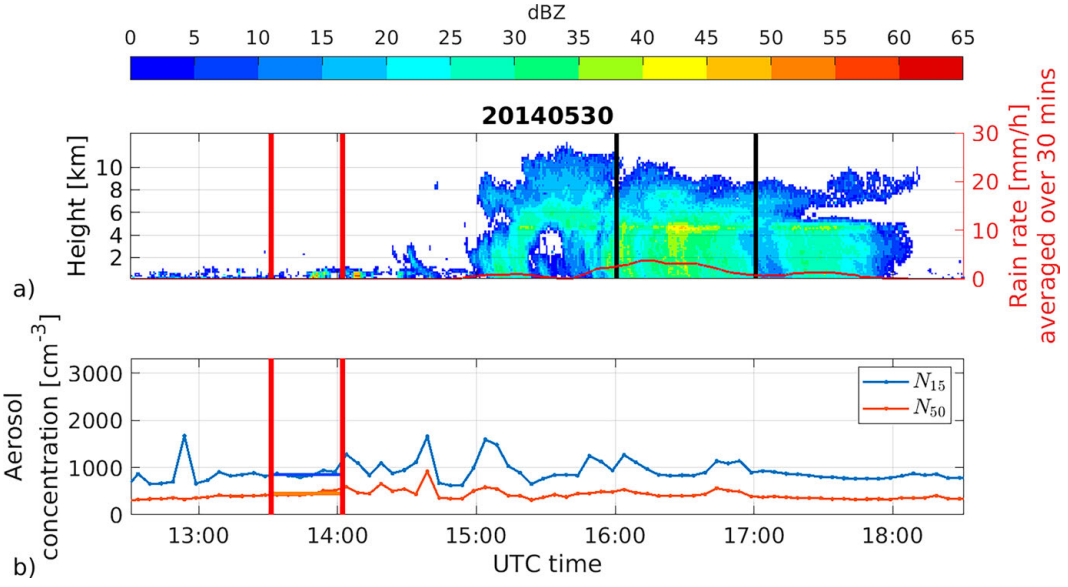

FIG. B5. As in Fig. 1, but for 30 May 2014.

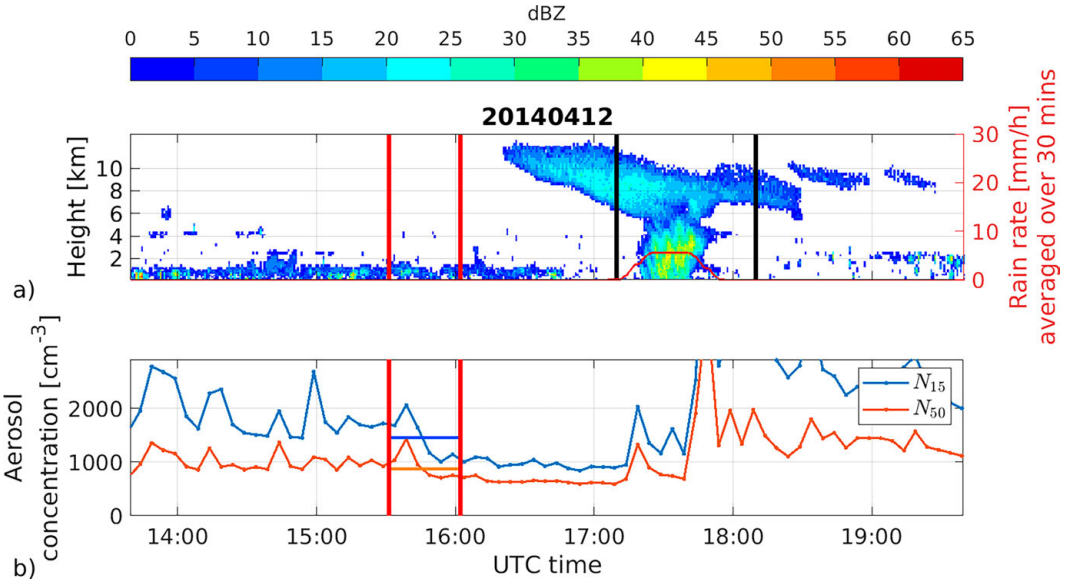

FIG. B6. As in Fig. 1, but for 12 Apr 2014.

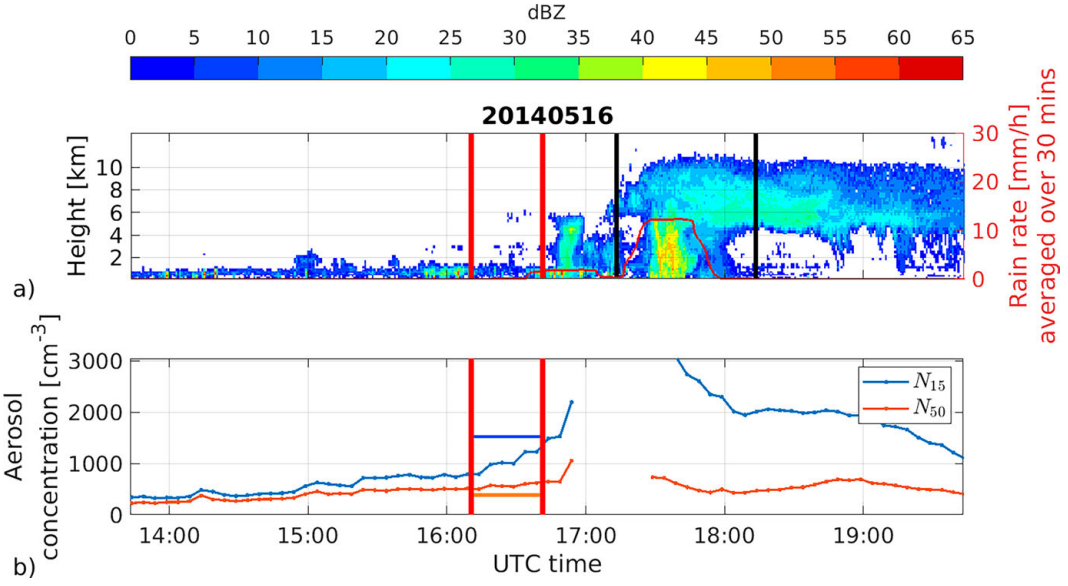

FIG. B7. As in Fig. 1, but for 16 May 2014.

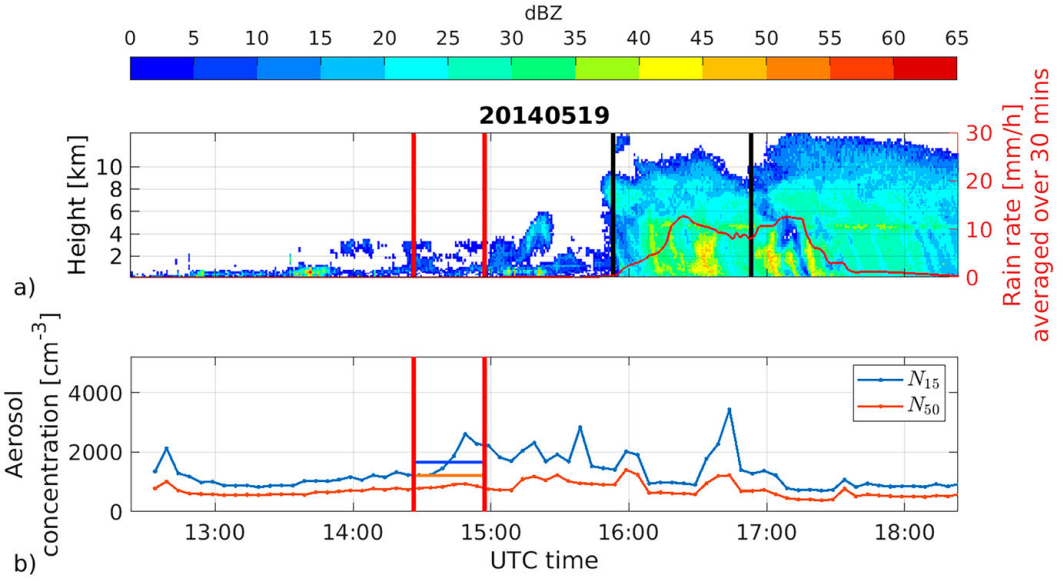

FIG. B8. As in Fig. 1, but for 19 May 2014.

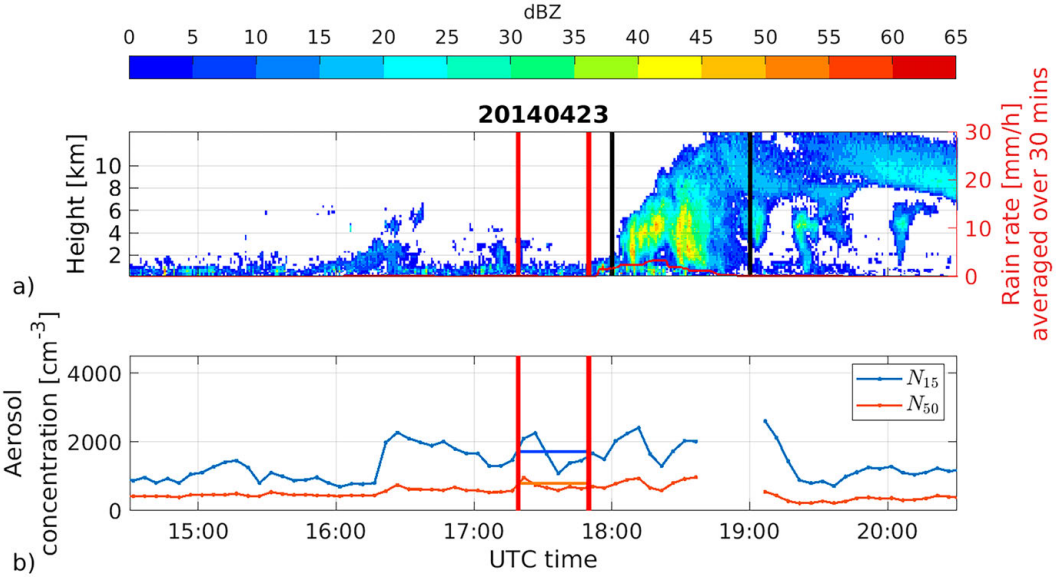

FIG. B9. As in Fig. 1, but for 23 Apr 2014.

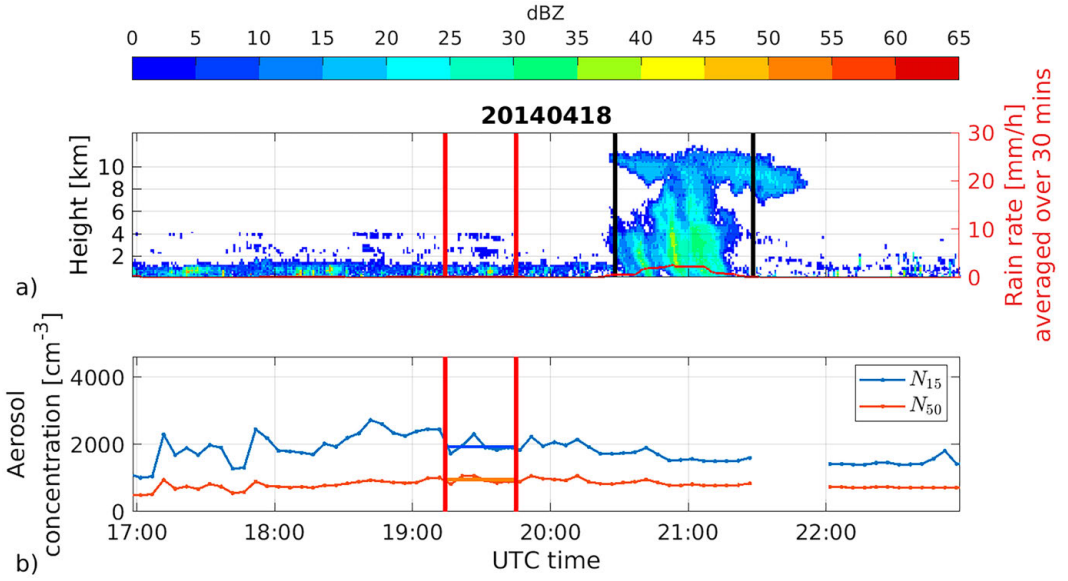

FIG. B10. As in Fig. 1, but for 18 Apr 2014.

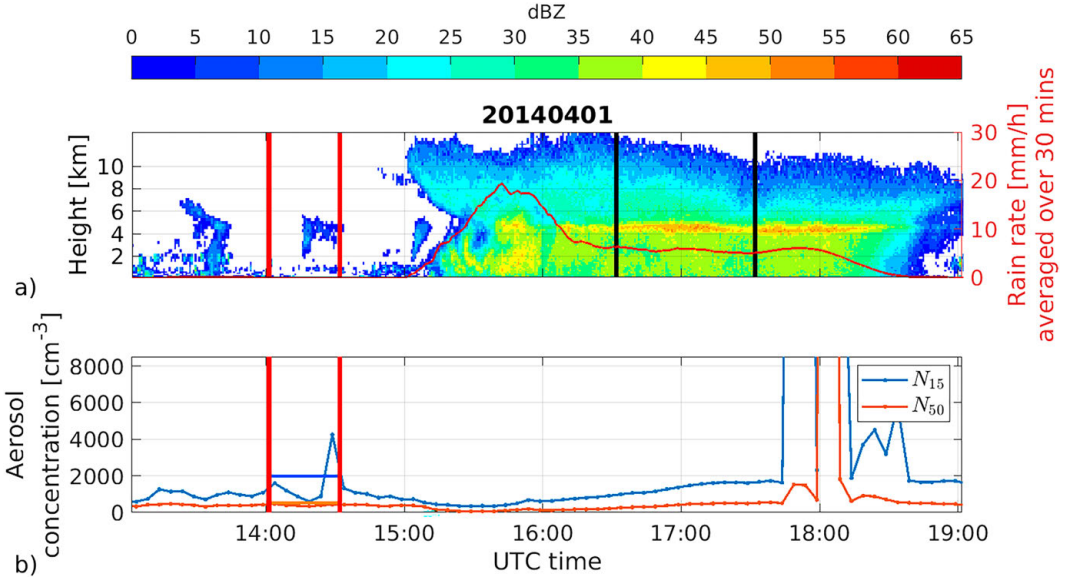

FIG. B11. As in Fig. 1, but for 1 Apr 2014.

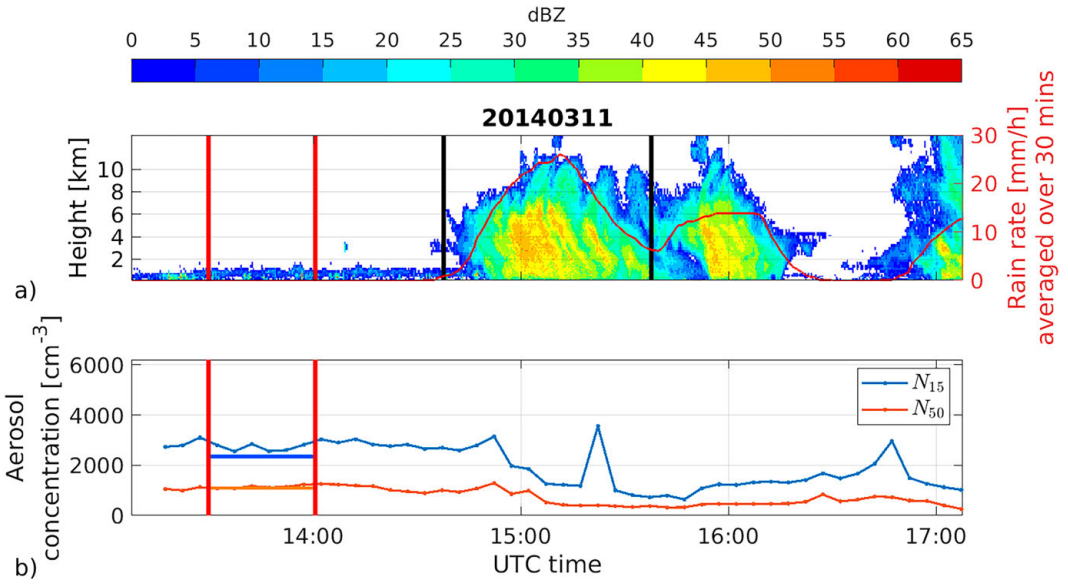

FIG. B12. As in Fig. 1, but for 11 Mar 2014.

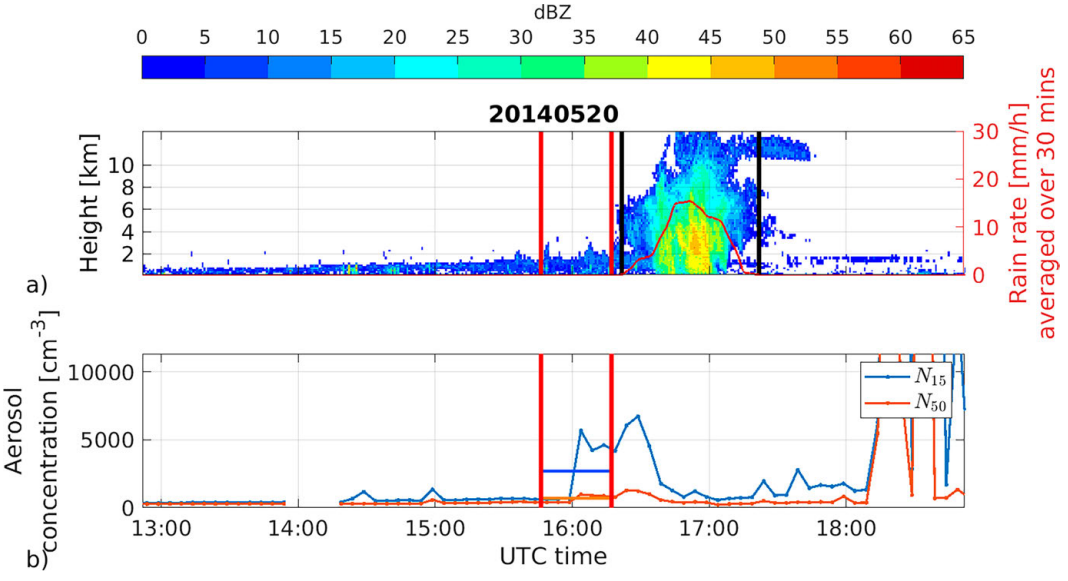

FIG. B13. As in Fig. 1, but for 20 May 2014.

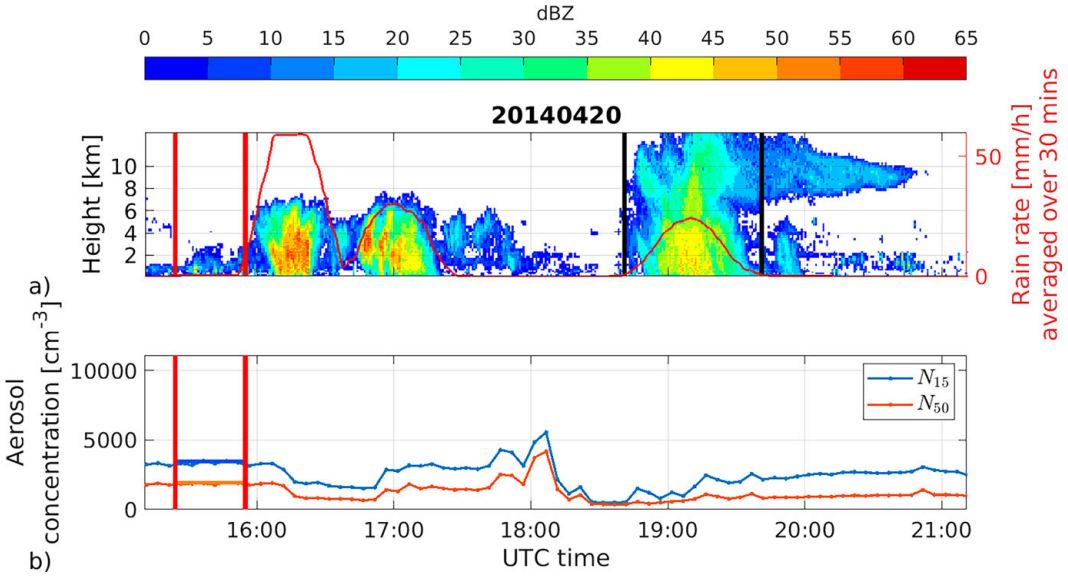

FIG. B14. As in Fig. 1, but for 20 Apr 2014.

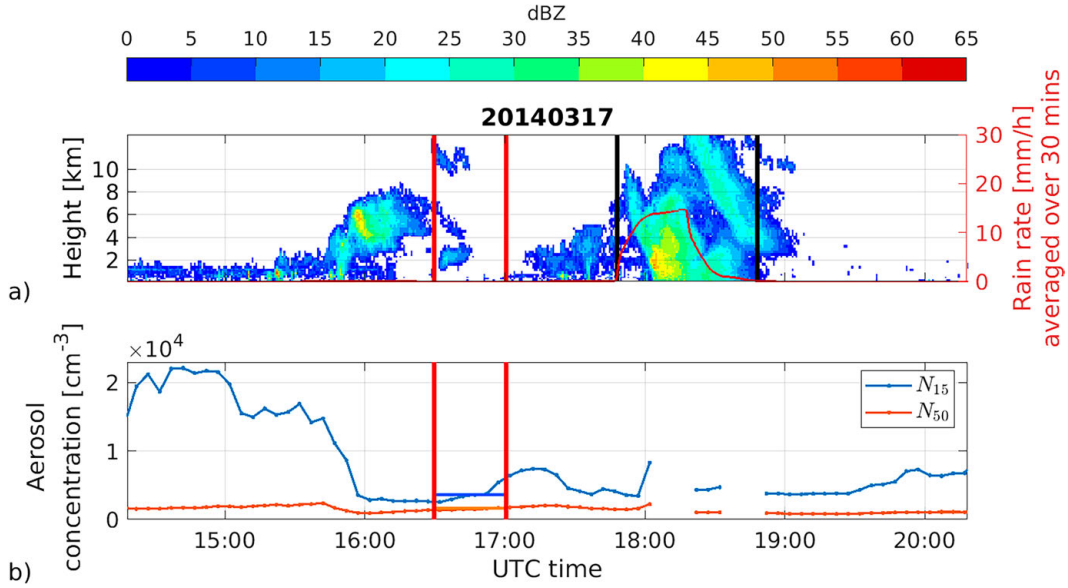

FIG. B15. As in Fig. 1, but for 17 Mar 2014.

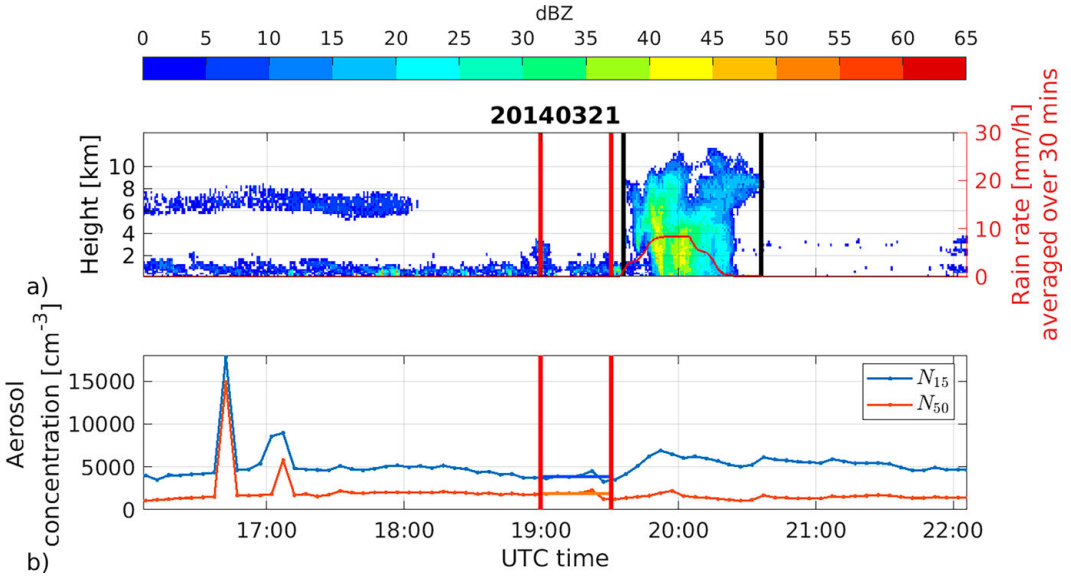

FIG. B16. As in Fig. 1, but for 21 Mar 2014.

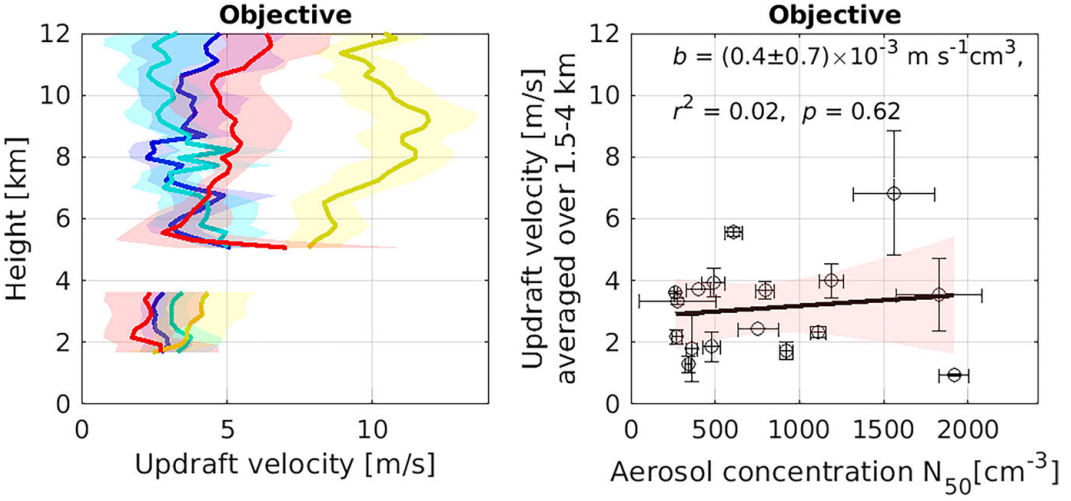

FIG. B17. As in Figs. 2c and 2f, but with the aerosol concentration represented by N_{50} instead of N_{15}. Following Fan18, the ranges of aerosol concentrations are $N_{50} < 500$ cm^{-3} (blue), $500 \le N_{50} < 1000$ cm^{-3} (cyan), $1000 \le N_{50} < 1500$ cm^{-3} (yellow), and $N_{50} \ge 1500$ cm^{-3} (red).

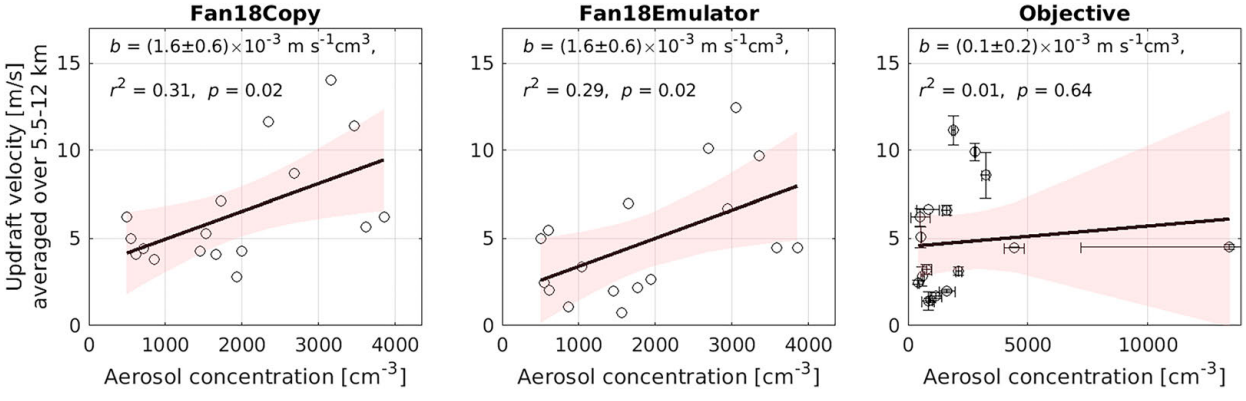

FIG. B18. As in Figs. 2d–f, but with updraft velocity averaged over upper troposphere.

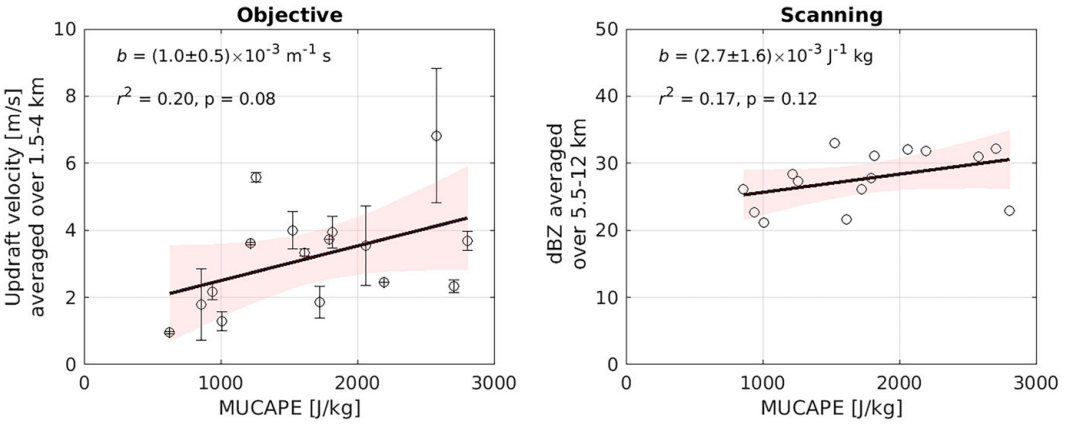

FIG. B19. (left) The Objective method's 90th-percentile velocity profile averaged over the lower troposphere (1.5–4 km), and (right) the 90th-percentile SIPAM reflectivity profile averaged over the upper troposphere, both plotted against MUCAPE from Table B1. The black lines show the linear least squares fit with the slope b, and the light red shading illustrates the 95% CI in the t test. The square of the Pearson correlation coefficient r^2 and the p value are printed at the top of the panels. The vertical error bars in the left panel correspond to standard deviations among the multiple parameter settings of the Objective tests.

TABLE B1. Convective available potential energy (CAPE-Fan18), most unstable convective available potential energy (MUCAPE), and convective inhibition (MUCIN). CAPE-Fan18 values are digitized from Fig. 2A of Fan18 and are from the nearest available radiosonde launch before each convective event. We calculated MUCAPE and MUCIN from the morning soundings at the same time on each day, removing sounding data below 10 m AGL due to suspiciously high temperature and dewpoint initializations that can bias CAPE and CIN values. There was no morning sounding on 18 Apr 2014.

Date	CAPE-Fan18 (J kg^{-1})	MUCAPE (J kg^{-1})	MUCIN (J kg^{-1})
23 Mar 2014	3643	1614	0
22 Mar 2014	3415	1216	6
21 Apr 2014	4419	937	9
31 May 2014	3202	1008	11
30 May 2014	3151	1724	1
12 Apr 2014	3584	2195	18
16 May 2014	5274	1816	6
19 May 2014	2358	2804	9
23 Apr 2014	2907	1295	34
18 Apr 2014	4348	—	—
1 Apr 2014	3202	858	8
11 Mar 2014	4419	2707	35
20 May 2014	3471	1790	20
26 Mar 2014	3702	1527	5
20 Apr 2014	3361	2578	7
17 Mar 2014	4564	2058	19
21 Mar 2014	3415	626	0

REFERENCES

Abbott, T. H., and T. W. Cronin, 2021: Aerosol invigoration of atmospheric convection through increases in humidity. *Science*, **371**, 83–85, https://doi.org/10.1126/science.abc5181.

Andreae, M. O., D. Rosenfeld, P. Artaxo, A. A. Costa, G. P. Frank, K. M. Longo, and M. A. F. Silva-Dias, 2004: Smoking rain clouds over the Amazon. *Science*, **303**, 1337–1342, https://doi.org/10.1126/science.1092779.

Cotton, W. R., and R. Walko, 2021: Examination of aerosol-induced convective invigoration using idealized simulations. *J. Atmos. Sci.*, **78**, 287–298, https://doi.org/10.1175/JAS-D-20-0023.1.

Fan, J., and Coauthors, 2009: Dominant role by vertical wind shear in regulating aerosol effects on deep convective clouds. *J. Geophys. Res.*, **114**, D22206, https://doi.org/10.1029/2009JD012352.

——, Y. Wang, D. Rosenfeld, and X. Liu, 2016: Review of aerosol–cloud interactions: Mechanisms, significance, and challenges. *J. Atmos. Sci.*, **73**, 4221–4252, https://doi.org/10.1175/JAS-D-16-0037.1.

——, and Coauthors, 2018: Substantial convection and precipitation enhancements by ultrafine aerosol particles. *Science*, **359**, 411–418, https://doi.org/10.1126/science.aan8461.

Giangrande, S., 2018: Calibrated radar wind profiler precipitation observations and vertical velocity retrievals. ARM, accessed 23 November 2021, https://doi.org/10.5439/1440997.

——, and Coauthors, 2016: Convective cloud vertical velocity and mass-flux characteristics from radar wind profiler observations during GoAmazon2014/5. *J. Geophys. Res. Atmos.*, **121**, 12 891–12 913, https://doi.org/10.1002/2016JD025303.

Grabowski, W. W., 2018: Can the impact of aerosols on deep convection be isolated from meteorological effects in atmospheric observations? *J. Atmos. Sci.*, **75**, 3347–3363, https://doi.org/10.1175/JAS-D-18-0105.1.

——, and H. Morrison, 2016: Untangling microphysical impacts on deep convection applying a novel modeling methodology. Part II: Double-moment microphysics. *J. Atmos. Sci.*, **73**, 3749–3770, https://doi.org/10.1175/JAS-D-15-0367.1.

——, and ——, 2020: Do ultrafine cloud condensation nuclei invigorate deep convection? *J. Atmos. Sci.*, **77**, 2567–2583, https://doi.org/10.1175/JAS-D-20-0012.1.

——, and ——, 2021: Supersaturation, buoyancy, and deep convection dynamics. *Atmos. Chem. Phys.*, **21**, 13 997–14 018, https://doi.org/10.5194/acp-21-13997-2021.

Hu, J., and Coauthors, 2019: Polarimetric radar convective cell tracking reveals large sensitivity of cloud precipitation and electrification properties to CCN. *J. Geophys. Res. Atmos.*, **124**, 12 194–12 205, https://doi.org/10.1029/2019JD030857.

Igel, A. L., and S. C. van den Heever, 2021: Invigoration or enervation of convective clouds by aerosols? *Geophys. Res. Lett.*, **48**, e2021GL093804, https://doi.org/10.1029/2021GL093804.

Khain, A. P., N. BenMoshe, and A. Pokrovsky, 2008: Factors determining the impact of aerosols on surface precipitation from clouds: An attempt at classification. *J. Atmos. Sci.*, **65**, 1721–1748, https://doi.org/10.1175/2007JAS2515.1.

Koren, I., Y. J. Kaufman, D. Rosenfeld, L. A. Remer, and Y. Rudich, 2005: Aerosol invigoration and restructuring of Atlantic convective clouds. *Geophys. Res. Lett.*, **32**, L14828, https://doi.org/10.1029/2005GL023187.

——, G. Feingold, and L. A. Remer, 2010: The invigoration of deep convective clouds over the Atlantic: Aerosol effect, meteorology or retrieval artifact? *Atmos. Chem. Phys.*, **10**, 8855–8872, https://doi.org/10.5194/acp-10-8855-2010.

Kuang, C., A. Singh, and J. Howie, 2021: Scanning mobility particle sizer (aossmps). ARM, accessed 14 October 2022, https://doi.org/10.5439/1476898.

Lebo, Z. J., 2014: The sensitivity of a numerically simulated idealized squall line to the vertical distribution of aerosols. *J. Atmos. Sci.*, **71**, 4581–4596, https://doi.org/10.1175/JAS-D-14-0068.1.

——, 2018: A numerical investigation of the potential effects of aerosol-induced warming and updraft width and slope on updraft intensity in deep convective clouds. *J. Atmos. Sci.*, **75**, 535–554, https://doi.org/10.1175/JAS-D-16-0368.1.

Li, Z., F. Niu, J. Fan, Y. Liu, D. Rosenfeld, and Y. Ding, 2011: Long-term impacts of aerosols on the vertical development of clouds and precipitation. *Nat. Geosci.*, **4**, 888–894, https://doi.org/10.1038/ngeo1313.

Martin, S. T., and Coauthors, 2016: Introduction: Observations and modeling of the Green Ocean Amazon (GoAmazon2014/5). *Atmos. Chem. Phys.*, **16**, 4785–4797, https://doi.org/10.5194/acp-16-4785-2016.

Romps, D. M., K. Latimer, Q. Zhu, T. Jurkat-Witschas, C. Mahnke, T. Prabhakaran, R. Weigel, and M. Wendisch, 2023: Air pollution unable to intensify storms via warm-phase invigoration. *Geophys. Res. Lett.*, **50**, e2022GL100409, https://doi.org/10.1029/2022GL100409.

Rosenfeld, D., U. Lohmann, G. B. Raga, C. D. O'Dowd, M. Kulmala, S. Fuzzi, A. Reissell, and M. O. Andreae, 2008: Flood or drought: How do aerosols affect precipitation? *Science*, **321**, 1309–1313, https://doi.org/10.1126/science.1160606.

Schumacher, C., and A. Funk, 2018: GoAmazon2014/5 three-dimensional gridded S-band reflectivity and radial velocity from the SIPAM Manaus S-band radar. ARM, accessed 23 November 2021, https://doi.org/10.5439/1459573.

Steiner, M., R. A. Houze Jr., and S. E. Yuter, 1995: Climatological characterization of three-dimensional storm structure from operational radar and rain gauge data. *J. Appl. Meteor.*, **34**, 1978–2007, https://doi.org/10.1175/1520-0450(1995)034<1978:CCOTDS>2.0.CO;2.

Stolz, D. C., S. A. Rutledge, and J. R. Pierce, 2015: Simultaneous influences of thermodynamics and aerosols on deep convection and lightning in the tropics. *J. Geophys. Res. Atmos.*, **120**, 6207–6231, https://doi.org/10.1002/2014JD023033.

Storer, R. L., S. C. Van den Heever, and T. S. L'Ecuyer, 2014: Observations of aerosol-induced convective invigoration in the tropical east Atlantic. *J. Geophys. Res. Atmos.*, **119**, 3963–3975, https://doi.org/10.1002/2013JD020272.

Tao, W.-K., J.-P. Chen, Z. Li, C. Wang, and C. Zhang, 2012: Impact of aerosols on convective clouds and precipitation. *Rev. Geophys.*, **50**, RG2001, https://doi.org/10.1029/2011RG000369.

Varble, A., 2018: Erroneous attribution of deep convective invigoration to aerosol concentration. *J. Atmos. Sci.*, **75**, 1351–1368, https://doi.org/10.1175/JAS-D-17-0217.1.

Yuan, T., L. A. Remer, K. E. Pickering, and H. Yu, 2011: Observational evidence of aerosol enhancement of lightning activity and convective invigoration. *Geophys. Res. Lett.*, **38**, L04701, https://doi.org/10.1029/2010GL046052.